Single-molecule analysis of solvent-responsive mechanically interlocked ring polymers and the effects of nanoconfinement from coarse-grained simulations *⊗*

Special Collection: Polymer Nanoconfinement

Diego Becerra (0); Alexander R. Klotz (0); Lisa M. Hall ■ (0)



J. Chem. Phys. 160, 114906 (2024) https://doi.org/10.1063/5.0191295







APL Machine Learning

2023 Papers with Best Practices in Data Sharing and Comprehensive Background

Read Now





Single-molecule analysis of solvent-responsive mechanically interlocked ring polymers and the effects of nanoconfinement from coarse-grained simulations

Cite as: J. Chem. Phys. 160, 114906 (2024); doi: 10.1063/5.0191295 Submitted: 12 December 2023 • Accepted: 2 March 2024 • Published Online: 21 March 2024















AFFILIATIONS

- William G. Lowrie Department of Chemical and Biomolecular Engineering, The Ohio State University, Columbus, Ohio 43210, USA
- ²Department of Physics and Astronomy, California State University, Long Beach, California 90840, USA

Note: This paper is part of the JCP Special Topic on Polymer Nanoconfinement.

- ^{a)}Electronic mail: diegobecerrariquelme@gmail.com. Current address: Department of Chemical Engineering, Universidad de Concepción, Concepción 4030000, Chile.
- b) Electronic mail: alex.klotz@csulb.edu
- c) Author to whom correspondence should be addressed: hall.1004@osu.edu

ABSTRACT

In this study, we simulate mechanically interlocked semiflexible ring polymers inspired by the minicircles of kinetoplast DNA (kDNA) networks. Using coarse-grained molecular dynamics simulations, we investigate the impact of molecular topological linkage and nanoconfinement on the conformational properties of two- and three-ring polymer systems in varying solvent qualities. Under good-quality solvents, for two-ring systems, a higher number of crossing points lead to a more internally constrained structure, reducing their mean radius of gyration. In contrast, three-ring systems, which all had the same crossing number, exhibited more similar sizes. In unfavorable solvents, structures collapse, forming compact configurations with increased contacts. The morphological diversity of structures primarily arises from topological linkage rather than the number of rings. In three-ring systems with different topological conformations, structural uniformity varies based on link types. Extreme confinement induces isotropic and extended conformations for catenated polymers, aligning with experimental results for kDNA networks and influencing the crossing number and overall shape. Finally, the flat-to-collapse transition in extreme confinement occurs earlier (at relatively better solvent conditions) compared to non-confined systems. This study offers valuable insights into the conformational behavior of mechanically interlocked ring polymers, highlighting challenges in extrapolating single-molecule analyses to larger networks such

Published under an exclusive license by AIP Publishing. https://doi.org/10.1063/5.0191295

I. INTRODUCTION

Linked-ring catenanes represent a class of polymers composed of two or more mechanically interlocked ring polymers.^{1,2} Theoretical, 3-5 computational, 5-14 and experimental 5,15-17 studies have extensively explored both typical ring polymers and their interlocked counterparts. It is challenging in general to synthesize compounds with specific topological linkages rather than typical covalent bonds.¹⁸ Notably, mechanically interlocked rings of DNA¹⁹ can be produced synthetically in multiple well-defined

topologies²⁰⁻²² to create structures with potential applications in switches and motors for molecular machines, owing to the mobility of the individual rings within the structure.²⁰⁻

Hierarchical structures composed of interlocking ring molecules also occur in nature, such as the networks of rings of DNA called kinetoplast DNA (kDNA) found in the mitochondria of trypanosome parasites, 17,27-40 with Crithidia fasciculata kDNA being the most studied variant.

This kinetoplast DNA is normally contained within a diskshaped organelle measuring 1 μm × 0.4 μm in vivo; 17 when

unconfined, the structure can be observed to form a "showercap" buckled shape of ~5 μ m. ^{29,41,42} Comprising about 5000 interlinked DNA "minicircles" (each containing 2500 base pairs, or 850 nm, long, and with low polydispersity⁴³) and a few dozen linked "maxicircles" (each containing 30 000 base pairs, or 10 μ m, long), containing the genetic information for the synthesis of mito-chondrial proteins. 31,39,44 While the structure of kDNA has been envisioned as uniform molecular chainmail^{27,28} with Hopf-linked minicircles forming a hexagonal network, detailed experimental observations and associated molecular simulations have provided a more complex view that these networks contain heterogeneities such as edges, holes, and additional links among some minicircles. 17 Other simulations provided detailed interpretations of experimental chromatography data, suggesting that rings in the network have a mean number of three links with other rings.^{27,45} It is also important to note that kDNA is distinctive for its lack of supercoiling, with the minicircles appearing relaxed when observed through electron microscopy. This case in the mitochondria of trypanosomatids could be unique, where covalently closed circular DNA is not supercoiled. Potentially, this factor promotes the formation of the kDNA network.46

Recent experimental advancements allow for the controlled deconstruction of the kDNA network⁴⁷ such that the remaining fragments can be carefully analyzed. Hopf links of two and three rings, as well as more intricate topological linkages involving four rings, have been observed.⁴⁷ An example that has not been directly observed in kDNA is Borromean rings, consisting of three mutually interconnected loops with no two loops sharing a direct binary link⁴⁸ (if one loop is broken, the other two become free of each other).

Because knots in polymers reduce the entropy of the knotted portion of the chain, entropy maximization favors the minimization of the contour length of the knotted portion, in an effect called self-tightening.⁴⁹ A similar effect can exist in linked systems, and Caraglio and colleagues in several studies showed that links tighten under confinement.

One can anticipate that a polymer ring's properties, especially conformational properties such as radius of gyration, could be impacted due to it being mechanically interlocked with other ring polymers instead of existing as an individual ring. These impacts, based on the imposition of topological constraints by other rings, could be considered local molecular confinement effects. In addition, in the realm of nanotechnological applications, these molecules can undergo overall molecular confinement in nanoslits or nanochannels, inducing anisotropy based on both the confinement geometry and the polymer's topological conformation. Prior work has shown conformational effects of confinement on individual rings that are different from those of linear polymers.⁵² It is also noteworthy that kDNA in slit-like confinement has been shown to somewhat unfold and adopt more uniformly circular shapes, in contrast to the more diverse conformations observed for kinetoplasts in bulk. 41 Previous simulation efforts have aimed to comprehend ring polymer chain behavior in slit-like confinement with various topological structures. These simulations primarily focus on the entropic force exerted by a dilute solution of ring polymer chains, featuring excluded volume interaction in a good solvent, on the confining parallel walls of the slit geometry, yielding a qualitative agreement with prior analytical results for ideal ring polymers.⁵³

Adding complexity to the structural analysis, the quality of the solvent in which these polymers are immersed plays a crucial role in their conformational properties.⁵⁴ In particular, for kDNA, networks composed of thousands of rings transition from a more flat phase (in a good solvent) to a collapsed phase (in a poor solvent), traversing an intermediate regime with varying shapes and sizes.³² While prior simulations have provided insights into the effect of catenation on the θ -temperature depression relative to ring and linear polymers,⁵⁵ our focus is on analyzing the influence of different topological links on conformations in good solvents and the flat-to-collapsed transition under varying degrees of confinement. Experiments examining crowding-induced³² and protein-induced⁴⁰ compaction of kDNA show that kinetoplasts can adopt much tighter configurations than those observed in good solvents. Experimental work by Holling⁵⁶ also indicates that similar condensation of kDNA networks, normally dispersed in water with varying amounts of salt, can be induced by mixing in ethanol, a poor solvent for DNA.

It is not fully understood what effect molecular topology has on solvent-induced collapse. It may be argued that, compared to an unentangled molecule of the same molecular weight, a knotted or linked molecule adopts a smaller conformation in the good solvent phase and a larger one in the poor solvent phase due to the persistent topological constraints, leading to a "softer" transition (with a smaller magnitude change in radius of gyration upon collapse). However, it is not known whether the number of entangled components or the complexity of each entanglement has a more significant effect or how these effects would interact to determine the behavior of a large catenated network.

In this study, we explore the impact of molecular topology and the effect of slit-like nanoconfinement on conformational properties under varying solvent qualities of fundamental catenanes comprising two and three rings. We focus on the Hopf-linked structures integral to kDNA and make comparisons to more highly linked or complex topological structures with otherwise comparable physical characteristics. Practical implications include an improved understanding of the conformations of the constituent components of kDNA, which is relevant in the interpretation of experimental realor inverse-space data on the size/shape of such components in a solution that may not have the resolution to detail the precise topology. However, our main objective is to glean fundamental insights into the intricate interplay of different types of confinement, topological, and solvent effects relevant to experimental systems.

This paper is organized as follows: We first discuss the selected topological links, our choice of a coarse-grained modeling approach, and the details of our simulation methodology in Sec. II. Section III is dedicated to presenting and discussing the conformational and structural outcomes when different topological links are subjected to varying solvent qualities and degrees of confinement. Finally, our findings are summarized in Sec. IV.

II. SIMULATION METHODS

A. Topological conformations

A prime link is mathematically defined as a link that cannot be represented as a sum of other links, while a composite link can be composed of combinations of other links. In this study, we consider prime links, as illustrated in Fig. 1. These links are designated by the

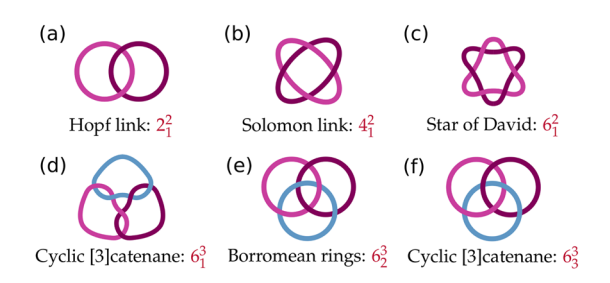


FIG. 1. Representation of linked-ring catenanes with topological isomerism in links considered in this study. Catenanes made up of two rings: (a) Hopf link (the simplest nontrivial link), (b) Solomon link, and (c) Star of David. Catenanes made up of three rings: (d) a certain cyclic [3]catenane, as shown, (e) Borromean rings, and (f) another cyclic[3]catenane with a different topological form. The links are listed by increasing complexity according to Rolfsen's table 58,59 and are labeled in red with the respective Alexander–Briggs notation, where a_c^b denotes the cth b-component link with crossing number a.

Alexander-Briggs notation, 57 denoted as a_c^b , and later extended by Rolfsen. 58,59 In this notation, a represents the minimum number of nodes or crossing points of any projection of the link, the superscript b is the number of linked components, and the subscript c is a conventional index to distinguish between topological isomers with the same number of nodes and linked components.

Figures 1(a)-1(c) show three prime links made up of two components (polymer rings in our case). These range from the elementary Hopf link (2_1^2) to the more intricate Star of David (6_1^2) , including the Solomon link (412). Considering slightly larger structures, we examine three prime links made up of three components or rings [see Figs. 1(d)-1(f)]: a cyclic [3]catenane (6_1^3) , where each ring is individually connected to the other two rings without shared links, the Borromean rings (6^3_2) , and the third cyclic [3]catenane in Rolfsen's table (6_3^3) . 6_1^3 and 6_3^3 represent the simplest closed Hopflinked chains but differ by a twist of the final loop. It was recently demonstrated14 that this twist chirality can have dramatic effects on the equilibrium configuration of polycatenanes. These topologies were chosen to allow us to examine the effect of both increasing the number of rings and the linkages per ring, as well as the effect of linking chirality. Although our current model does not include local nonisotropic interactions or torsions, there is no energy penalty for twisting as there would be in real DNA. As baseline cases, we have also studied the conformation of a single isolated ring to demonstrate the specific impact of the topological linkage and a single linear polymer chain for comparative purposes.

B. Coarse-grained model

Our coarse-grained model is based on the physical properties of kDNA minicircles that can be experimentally isolated outside the kDNA network. 17,47 Each polymer ring in our systems is made of bonded beads of size σ [where size refers to the Lennard-Jones (LJ) diameter with the potential given below]. We set $\varepsilon = \sigma = m$ to unity for all beads (these are our reduced LJ units of energy, length, and mass). In physical units, the hydrated diameter of doublestranded DNA is 2.5 nm, and its persistence length is approximately $l_p \simeq 50$ nm. Mapping the bead diameter to SI units (nm), we set σ = 2.5 nm. The contour length for each polymer ring should be

 $L_c \sim 340\sigma = 850 \text{ nm} \simeq 2.5 \text{ kbp } (\sim 17 l_p \text{s long})$. Therefore, the persistence length is set to $l_p = 20\sigma$ by adding the angle potential described below. We simulate different systems, each considering one of the topological conformations shown in Fig. 1, where each ring has a total of 340 monomer beads. Consequently, there are a total of 680 beads in two-ring systems and 1020 beads in three-ring systems.

In particular, the polymer rings are modeled with a standard Kremer-Grest (KG) bead-spring model. 60,61 Successive beads in the ring are connected by the finitely extensible nonlinear elastic (FENE) potential combined with the repulsive portion of the LJ potential [the Weeks-Chandler-Andersen (WCA) potential], 62,63

$$U_{\text{bonded}}(r_{i, i+1}) = U_{\text{FENE}}(r_{i, i+1}) + U_{\text{WCA}}(r_{i, i+1})$$

$$= -\frac{1}{2}k_{\text{FENE}}R_0^2 \ln\left[1 - \left(\frac{r_{i, i+1}}{R_0}\right)^2\right]$$

$$+ 4\varepsilon\left[\left(\frac{\sigma}{r_{i, i+1}}\right)^{12} - \left(\frac{\sigma}{r_{i, i+1}}\right)^6\right] + \varepsilon, \qquad (1)$$

where $r_{i,i+1}$ is the distance between the two beads, $k_{\text{FENE}} = 30k_{\text{B}}T/\sigma^2$ is the spring constant, and $R_0 = 1.5\sigma$ is the maximum extent of the bond where the FENE potential diverges. The second term is the WCA potential and is cut off at $r_c = 2^{1/6}\sigma$, the minimum of the full LJ potential. The parameters used here have been shown to energetically prevent bonds from crossing and, therefore, enforce the mechanical bonds, which are specified entirely by the initial conditions of the simulations. The average bond length is $\langle l \rangle \equiv 0.965\sigma$. Note that we consider torsionally relaxed DNA rings with no twist, as shown in Refs. 17 and 45.

To model interactions between nonbonded particles and account for the influence of an implicit solvent, it is essential to consider solvent-mediated interactions that induce correlations between segments along the chain. In this study, we employed a tunable potential represented as a piecewise function of repulsive and attractive parts, ensuring continuity at r_c for $r_c > 2^{1/6}\sigma$ as shown in Refs. 12 and 64. In this context, the repulsive portion has the same shape while the attraction is added with strength based on the parameter λ . In particular,

$$U_{\text{nonbonded}}(r_{ij}) = \begin{cases} 4 \varepsilon \left[\left(\frac{\sigma}{r_{ij}} \right)^{12} - \left(\frac{\sigma}{r_{ij}} \right)^{6} \right] + \varepsilon (1 - \lambda), & r_{ij} \leq 2^{1/6} \sigma, \\ 4 \varepsilon \lambda \left[\left(\frac{\sigma}{r_{ij}} \right)^{12} - \left(\frac{\sigma}{r_{ij}} \right)^{6} \right], & r_{ij} > 2^{1/6} \sigma, \end{cases}$$
(2)

where r_{ij} is the distance between two nonbonded beads, i and j. As mentioned earlier, the parameter λ controls the depth of the attractive well, which accounts for the overall effect of the solvent implicitly. (No attraction between monomers, λ of zero, implies the athermal, good solvent case where effects of monomer-monomer, monomer-solvent, and solvent-solvent interactions cancel overall, and it is not preferable that monomers interact with each other over the solvent, which is not explicitly represented. Put another way, in this limit, if our slightly soft repulsive potential is approximated as perfectly hard, there would be no internal energy change in mixing a monomer fluid and solvent. A greater attraction between monomers implies that monomer-monomer or solvent-solvent interactions

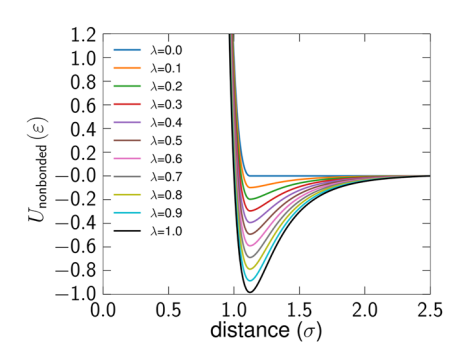


FIG. 2. Effective nonbonded interaction curves with different λ values representing varying solvent qualities.

are relatively more favorable, corresponding to poorer solvents).⁶⁴ The influence of different λ values on the nonbonded potential is illustrated in Fig. 2; here, we explore values of λ ranging from 0 (athermal solvent) to 0.6, which is below the collapse threshold for our systems. Note that we truncated and shifted the pairwise potential of Eq. (2) at a cutoff of 2.5σ .

To set the persistence length of the model, we used the Kratky-Porod potential as in prior work, 17,

$$U_{\text{bend}}(\theta) = k_{\text{B}} T l_p / \sigma (1 + \cos \theta), \tag{3}$$

where θ is the angle between three consecutive beads along the chain and the bending energy $k_{\rm B}Tl_p/\sigma \equiv k_{\rm bend} = 20k_{\rm B}T$.

C. Langevin dynamics

Because our systems are in an implicit solvent, we use a Langevin thermostat that includes a random noise term (Langevin dynamics) to simulate the canonical ensemble at constant $T = 1.0\varepsilon/k_{\rm B}$. Therefore, given the positions of each bead i and the conservative forces $F_{c,i}(t)$ based on the gradient of all pairwise potentials from Eqs. (1)-(3), the time evolution of the beads is governed by the Langevin equation,

$$m\frac{d^2\mathbf{r}_i}{dt^2} = \mathbf{F}_{c,i} - \zeta \frac{d\mathbf{r}_i}{dt} + \mathbf{W}_i(t), \tag{4}$$

where m is the bead's mass and ζ is the friction coefficient set to $\zeta = 0.5m/\tau$, where $\tau = \sigma \sqrt{m/\varepsilon} = 1$ is the characteristic time unit of the simulation. 11,61,65,66 The friction coefficient, ζ , is related to the damping factor, τ_m , in the implementation of the Langevin thermostat by $\zeta = (m/\tau_m)$. $W_i(t)$ is a random force with Gaussian white noise statistics obeying $\langle W_i(t) \rangle = 0$ and $\langle W_i(t) W_i(t') \rangle$ = $2\zeta m k_{\rm B} T \delta_{ij} I \delta(t-t')$, where δ is the Dirac delta function and I is the identity matrix. This strategy implies that, on average, the stochastic fluctuations are balanced by the dissipative forces, and the overall energy stays approximately constant. We use the opensource LAMMPS package⁶⁷ to perform the simulations with a time step of 0.005τ .

D. Simulation setup

We perform single-molecule simulations of the six catenane systems shown in Fig. 1, where different values of λ ranging from 0.0 to 0.6 (the collapse threshold for our systems) are considered. The initial configuration for each system was created using the software Avogadro,68 followed by an energy minimization of the system. In addition, certain systems underwent a slit-like nanoconfinement effect, detailed below.

To address confinement, it is crucial to note that a linear polymer chain with a persistence length l_p undergoes deformation when confined to a geometry where at least one dimension d is smaller than the equilibrium size in bulk $(R_{g,\text{bulk}})$. This results in distinct regimes, such as the de Gennes regime⁶⁹ $(R_{g,\text{bulk}} > d \gg l_p)$ and the Odijk regime⁷⁰ ($l_p \gg d$), each influencing the physical properties of the polymers.

For simulations without slit-like confinement, a cubic simulation box with constant volume and periodic boundary conditions of dimensions $(300 \times 300 \times 300)\sigma^3$ is employed to prevent catenanes from interacting with themselves through the boundaries. For simulations with slit-like confinement, we implemented repulsive walls, confining the catenane molecule with a height $h = 5\sigma$ along the z-axis of the computational box. This condition represents extreme confinement since the confining dimension is smaller than the persistence lengths of the molecules studied; in particular, $h = 5\sigma$ corresponds to ~12.5 nm in real units for DNA, which is in the Odijk regime. The walls interact with catenane beads using the repulsive WCA potential (Lennard-Jones 12-6 cutoff and shifted at $r_c = 2^{1/6}\sigma$), generating a force on the atoms perpendicular to the wall. In these cases, the computational box is periodic only in the directions parallel to the walls (x- and y-directions of the computational box) and is constrained by confining walls in the z-direction.

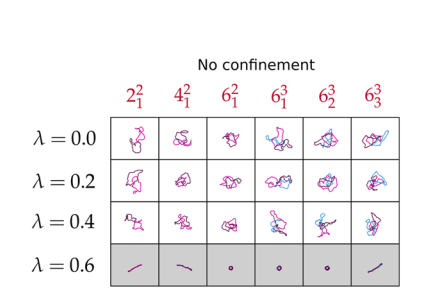
Systems are then equilibrated for a total time of $1 \times 10^7 \tau$ to achieve an equilibrium conformation and decorrelation in the position of beads.

After equilibration, all systems underwent a production run lasting at least 1×10^9 time steps, equivalent to $5 \times 10^6 \tau$, as described in Ref. 71, for measuring conformational properties.

III. RESULTS AND DISCUSSION

To initiate the analysis and adopt a more intuitive approach, first visually inspect representative snapshots from molecular dynamics (MD) simulations, as depicted in Fig. 3, for all systems studied under varying solvent qualities and for both nonconfined conditions and under slit-like confinement. Note that each configuration is presented on the same scale for a clear comparison in terms

Upon initial examination, it is observed that structures collapse under poor enough solvent conditions in both non-confined and slit-like confinement systems. This occurs when the interaction parameter λ reaches 0.6 for non-confined systems and 0.4 for confined systems (note we only consider increments of 0.2λ in this work, so we are unable to determine the exact transition point, although we plan to consider finer changes in solvent quality in future work). Morphologically, the collapsed structures vary based on the type of links. Another visually notable characteristic is that under nanoconfinement, structures are more extended in the plane perpendicular to the confinement direction and appear more radially symmetric compared to the same structures under non-confined conditions. This



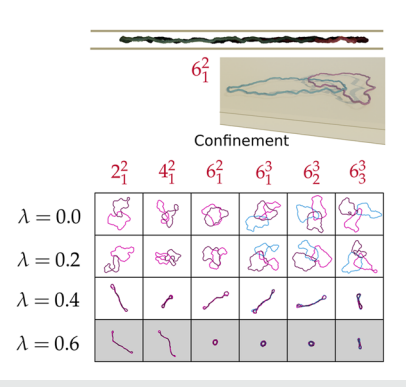


FIG. 3. Representative snapshots of linked-ring systems with various topological conformations (labeled with Alexander–Briggs notation⁵⁷ in red) under varying solvent qualities for nonconfined conditions (left) and in slit-like confinement (right). In the case of slit-like confinement, a front view is provided along with a perspective from an oblique top view for the 6_1^2 molecule for illustrative purposes. (The gray background for systems with $\lambda=0.6$ indicates potential kinetically trapped states, which might not persist indefinitely. The data in this case are only provided for completeness.)

behavior is intuitively expected and similar to experimental observations of larger kDNA networks, in which flattened quasi-2D shapes were observed under extreme confinement.⁴¹

At low λ values of 0.0 and 0.2 (good solvent conditions), the analysis of two-ring systems reveals that a higher number of nodes or crossing points in any link projection results in a more internally constrained structure and a smaller average size under these conditions. This is evident in both non-confined and nanoconfined systems. Crossing points in these systems are distributed along the ring domains, preventing them from moving far from each other as the number of links increases, as shown in the $6\frac{1}{1}$ system.

Interestingly, at low λ values of 0.0 and 0.2, the three-ring systems all appear to be of similar size, at least visually. This may be because, in contrast to the two-ring systems, all of the three-ring systems have the same crossing number. For the studied types of three-ring systems, the rings can move away from each other, concentrating the links near a common point in the middle. This can be better appreciated in confined systems.

For higher λ values, confined structures collapsed before (at a more modest λ or not as poor solvent quality) non-confined systems. This is expected because these systems have less conformational entropy in the non-collapsed state due to their confinement and so lose less entropy upon collapse (while one expects they have a similar amount of energy upon collapse as non-confined systems, overall making collapse more favorable), and similar effects have also been observed experimentally for confined DNA. For confined systems and $\lambda=0.4$, all the topological links under study exhibit similar rod-like collapsed conformations that are more than one chain segment thick and relatively extended along one dimension. At $\lambda=0.6$, both confined and non-confined systems are collapsed, and two particular conformations can be observed: rod-like structures and small toroid-like structures, both of which are multiple segments thick.

We believe these result from competing energetic effects: (1) the systems would tend to collapse into structures that are overall more compact/spherical and have more local contacts (LJ interactions), but (2) there is also an energetic penalty for chain bending (due to the angle potential). Chains can increase their interactions

with less bending if they align locally so that relatively straight local regions of the chains can interact with each other. Depending on the topology and bending penalty relative to solvent strength, as well as the initial state and how exactly it evolves toward a collapsed structure over time, the system may coil into a toroidal shape with a locally consistent bending that is less than that required to fully fill a spherical shape, vs creating a rod-like structure with mostly straight regions and a smaller number of bent angles near the ends. We note that the systems at $\lambda = 0.6$ are kinetically trapped (they are not able to explore other conformations after collapsing quickly during the beginning of the simulation), and different states (rod-like vs toroid-like) can evolve from different random initial conditions for some of these systems, as shown in the supplementary material. While these observed states may provide insight into the possible experimentally relevant kinetically trapped states, we make no attempt to simulate specific cooling or solvent exchange processes, and thus, we do not address the likelihood of the systems forming these particular collapsed states experimentally. Below, we show the results for these states at $\lambda = 0.6$ for completeness and to highlight the fact that the systems all reach a collapsed state at high λ , but we do not focus on which type of collapsed state they form under this condition.

To quantitatively characterize the structural features of our linked-ring catenane systems under varying solvent conditions and degrees of confinement, we calculated the gyration tensor, denoted as G. Each component of the gyration tensor is defined as

$$G_{\alpha\beta} = \frac{1}{N_b} \sum_{i=1}^{N_b} \langle r_{i, \alpha} r_{i, \beta} \rangle, \tag{5}$$

where N_b is the total number of beads, $r_{i,\alpha}$ is the position of bead i relative to the catenane molecule's center of mass, and $\alpha, \beta \in \{x, y, z\}$. The gyration tensor is a symmetric 3×3 matrix, and its eigenvectors are the principal axes of the shape (if the shape is rotated to this coordinate system, G is a diagonal matrix of eigenvalues). We define the eigenvalues, sorted in descending order, as λ_x^2 , λ_y^2 , and

 $\lambda_z^2~(\lambda_x^2 \geq \lambda_y^2 \geq \lambda_z^2)$. This convention makes it so that each λ_α has length units and is the same as the one dimensional radius of gyration calculated along the corresponding principal axis; the overall squared radius of gyration, R_g^2 , is tr $G=\lambda_x^2+\lambda_y^2+\lambda_z^2$. For each shape, the eigenvalues (and the differences in centers of mass of rings and crossing numbers as discussed below) are computed at each saved configuration in time, then each is averaged over time before being used to calculate further quantities given below, such as R_g^2 .

In Fig. 4(a), for systems under no confinement, R_g values are approximately constant as a function of λ when $\lambda \leq 0.4$, then decrease significantly when the systems are collapsed at $\lambda = 0.6$. In the case of two-ring systems, the largest R_g is for the Hopf link 2_1^2 , followed by the Solomon link 4_1^2 , with the smallest being the Star of David 6_1^2 . Thus, in agreement with expectations and the visual inspection in Fig. 3, the increased complexity of the topological linkage leads to a smaller R_g for two-ring systems. However, in the case of three-ring systems, the opposite is observed. Here, the 6_3^3 system, which has the highest complexity, shows the largest R_g , although the differences between values for three-ring systems are relatively small. Note that in this regime, the Hopf-linked three-ring systems $(6_1^3$ and 6_3^3) lie at similar values to the single Hopf link molecule (2_1^2) .

On the other hand, for $\lambda = 0.6$, where all structures collapse, the systems take on one of two R_g values related to the two types of conformations discussed above: rod-like structures $(2_1^2, 4_1^2, \text{ and } 6_3^3)$ with a higher R_g value) and toroid-like structures $(6_1^2, 6_1^3, \text{ and } 6_2^3)$ with a smaller R_g value).

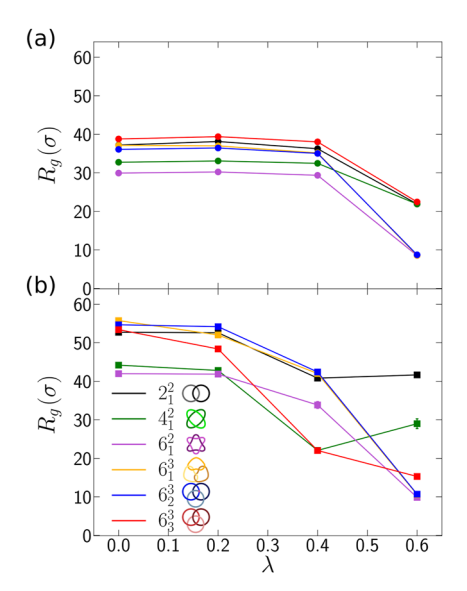


FIG. 4. Mean radius of gyration, R_g , as a function of the interaction parameter λ for various topological conformations (labeled with Alexander–Briggs notation⁵⁷) (a) without confinement and (b) in slit-like confinement. The bars show the standard errors of all the measurements (note that the error bars are smaller than the symbols). Note that $\lambda=0.6$ results are presented only for completeness; those systems are collapsed into compact shapes that are kinetically trapped in a certain way depending on the initial conditions and do not represent equilibrium states.

The R_g values of systems under slit-like confinement, as shown in Fig. 4(b), vary differently and are, in general, larger than those of non-confined systems. For $\lambda=0.0$ and 0.2, we observe that systems 4_1^2 and 6_1^2 are significantly smaller than the rest; while most systems can concentrate all their crossings near one point and spread out otherwise, these 4_1^2 and 6_1^2 systems are more internally constrained and, thus, remain smaller. Note that, in contrast to the non-confined systems, the confined systems become slightly smaller at $\lambda=0.2$ and significantly smaller at $\lambda=0.4$, at which point the non-confined systems have not yet collapsed, as observed in Fig. 3. At $\lambda=0.6$, the systems are collapsed into qualitatively similar overall structures to their non-confined counterparts, although their R_g values can be different depending mostly on the thickness of the structures.

As baseline cases, we simulated a single isolated ring under varying solvent conditions and also a single linear polymer chain for comparative purposes (see Fig. S1 in the supplementary material). At first glance, for the non-confined isolated ring [Fig. S1(a)], a small and constant value of R_g is observed until $\lambda = 0.4$, which is expected since it is a single ring and comparable to the value of the 6_1^2 structure. In the case of slit-like confinement, interestingly, the same bulk trend and values for the isolated ring are practically maintained, with no abrupt decay at $\lambda = 0.4$ as observed in all catenanes studied under slit-like nanoconfinement [see Fig. 4(b)] and also in the case of the linear polymer chain, which shows a more similar trend to catenanes under extreme confinement in terms of R_g trends.

It is instructive to decompose the measurements for R_g and analyze the biggest and smallest eigenvalues separately (see Fig. 5) to compare how relatively extended each shape is along its long axis or shortest dimension.

In non-confined systems, at low λ values, trends in both the largest and smallest eigenvalues [see Figs. 5(a) and 5(b), respectively] are consistent with the R_g measurements shown in Fig. 4. However, the differences in the collapsed values at high λ (poorquality solvent) are primarily dictated by the largest eigenvalues (all non-confined collapsed systems' smallest eigenvalues are similar); the largest eigenvalue primarily indicates whether the system happened to become trapped in a long rod-like state or a more compact toroid-like state. Under slit-like confinement [see Figs. 5(c) and 5(d)], the trends in the largest eigenvalues with respect to system type and solvent quality are generally the same as those seen from the R_g measurements. Of course, the smallest eigenvalue for these systems is always relatively small due to the confinement in one dimension. Note that monomers occupy a restricted height due to confinement between approximately -1.5σ and 1.5σ , with 0 representing the midpoint of the repulsive walls implemented. The wall's location is set at where the potential diverges; the center of a bead at the point where there is a $1k_BT$ energy penalty for being near the wall is at σ , making the effective distance between walls for beads' centers to exist about 3σ . They experience zero repulsive force only in the middle region of $5-2\times2^{1/6}$ = 2.76 σ . Interestingly, the four systems with the lowest λ_x^2 values $(6_1^2, 6_1^3, 6_2^3, \text{ and } 6_3^3)$ exhibit somewhat larger λ_z^2 values (although these are still extremely small relative to the extension in other directions). This is indicative of thicker configurations in which segments are partly stacked on top of each other in the direction of confinement.

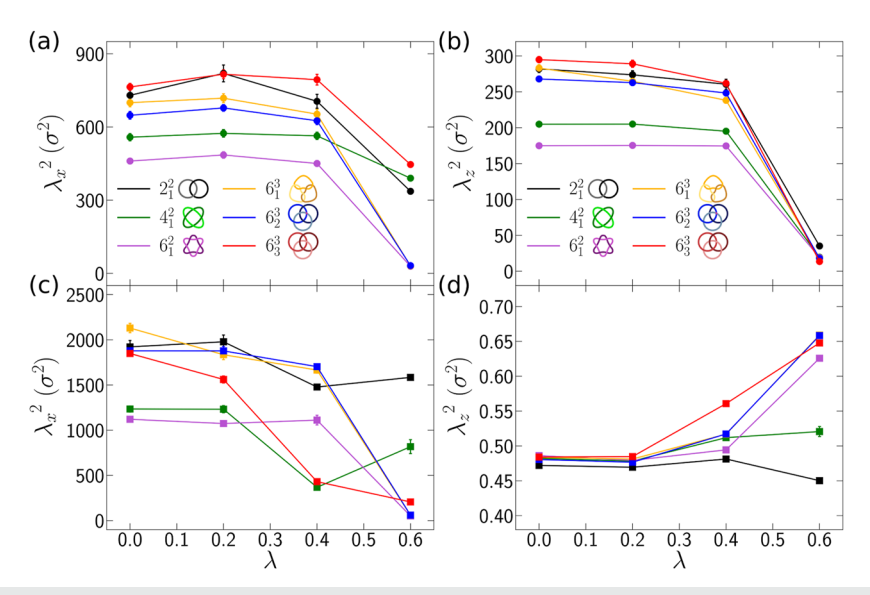


FIG. 5. (a) Biggest and (b) smallest eigenvalues of the gyration tensor (\mathbf{G}) as a function of the interaction parameter λ for various topological conformations (labeled with Alexander–Briggs notation⁵⁷) in systems without confinement. (c) Biggest and (d) smallest eigenvalues of the gyration tensor (\mathbf{G}) as a function of the interaction parameter λ for various topological conformations (labeled with Alexander–Briggs notation⁵⁷) in systems with slit-like confinement. The bars show the standard errors of all the measurements (note that the error bars are smaller than the symbols). Note that $\lambda = 0.6$ results are presented only for completeness; those systems are collapsed into compact shapes that are kinetically trapped in a certain way depending on the initial conditions and do not represent equilibrium states.

We also quantify the polymer conformation by monitoring the relative shape anisotropy, κ^2 , defined by

$$\kappa^2 := \frac{3}{2} \frac{\lambda_x^4 + \lambda_y^4 + \lambda_z^4}{(\lambda_x^2 + \lambda_y^2 + \lambda_z^2)^2} - \frac{1}{2},\tag{6}$$

where $0 \le \kappa^2 \le 1$. A perfect sphere has $\kappa^2 = 0$, while a one dimensional rod has $\kappa^2 = 1$, a limit that is not possible for these ring systems. For planar, circularly symmetric objects, the relative shape anisotropy converges to the value of 1/4. The shape anisotropy calculated for all the systems studied is shown in Fig. 6.

For non-confined systems [Fig. 6(a)], a constant trend is observed for all systems, with $\kappa^2 \leq 0.11$ until just before the structures collapse, indicating relative isotropy in the 3D configurational space.

For confined systems [Fig. 6(b)], at $\lambda=0$ and 0.2, all values are between 0.3 and 0.4 because they are spread or extended (but not completely symmetrically) across the plane perpendicular to the confinement direction, exhibiting κ^2 values slightly higher than 0.25. The highest κ^2 value among the systems is for the 2_1^2 configuration, owing to its having only one Hopf link, making it less symmetrical in the x-y plane than three-ring systems. It is noteworthy that under confinement, a flat-to-collapse transition is induced at $\lambda \sim 0.4$ (which is before the collapse transition for non-confined systems), which increases κ^2 . At this point, all confined systems visually appear rod-like, although the value of κ^2 is somewhat different across the systems. At $\lambda=0.6$, all systems are more significantly locally collapsed.

To explore how the topological linkage impacts the asymmetry between rings within a catenane molecule under varying solvent

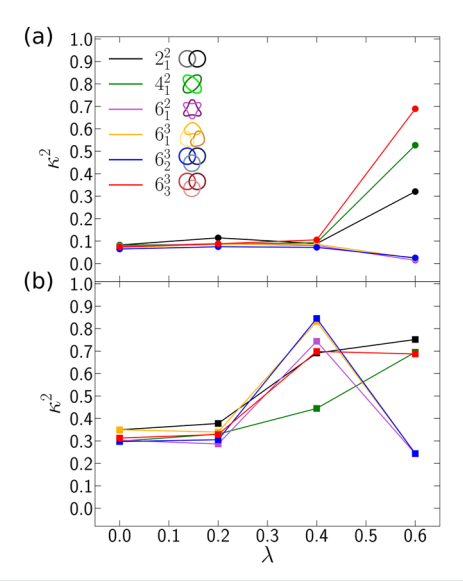


FIG. 6. Relative shape anisotropy, κ^2 , as a function of the interaction parameter λ for various topological conformations (labeled with Alexander–Briggs notation⁵⁷) (a) without confinement and (b) in slit-like confinement. Note that $\lambda=0.6$ results are presented only for completeness; those systems are collapsed into compact shapes that are kinetically trapped in a certain way depending on the initial conditions and do not represent equilibrium states.

qualities, Fig. 7 presents the time-averaged absolute percentage difference in R_g (ΔR_g) of the larger/largest and smaller/smallest rings in two-ring/three-ring systems for both confined and non-confined systems. In addition, Fig. 7 shows the mean-squared center-to-

center distance between interlocked rings, L^2 , normalized by the mean squared radius of gyration of the molecule $(R_{\rm g}^{\ 2})$, for both non-confined and confined systems. In particular, the mean-squared center-to-center distance measurements consider the average distance between centers of mass of two rings; for three-ring systems, the measurements are averaged across all possible two-ring combinations.

For non-confined systems, ΔR_g values plateau at low values of λ ($\lambda \leq 0.4$) for all the systems [see Fig. 7(a)]. Notably, the system with the lowest ΔR_g value, 2_1^2 , results from only one constraint acting equivalently on both rings. On the other hand, differences are larger in three-ring systems.

In confined systems [see Fig. 7(c)] with low λ values (0 and 0.2), certain configurations, such as 2_1^2 , 6_1^2 , and 6_2^3 , show very small ΔR_g . In the cases of 2_1^2 and 6_2^3 , there is only one link, or the links can be brought to a single small region, such that the rest of the rings can each extend relatively independently in a similar shape to the others. The reason for the small ΔR_g for the 6_1^2 may be different because the many links between only two rings mean that the links stay evenly distributed, keeping the rings similar to each other. The other systems, 4_1^2 , 6_1^3 , and 6_3^3 , exhibit higher ΔR_g values as their links and conformations are apparently not even within the molecule.

In Fig. 7(b), the normalized mean-squared center-to-center distances of the interlocked rings, L^2/R_g^2 , are shown for non-confined conditions. The trends are similar for all the systems studied, with a plateau for $\lambda \leq 0.4$ (albeit at different values) and a common collapse point for all configurations. For two-ring systems, the more required crossings, the lower the L^2/R_g^2 value (the closer the rings are, as one would expect). Interestingly, for three-ring systems, different values are also observed at low λ values, although the number of crossings

is the same. This indicates that the topological linkage type plays a significant role in the conformational properties of the molecules. Here, the 6^3_3 configuration exhibits the highest L^2/R_g^2 value due to the concentration of all crossings in the middle, enabling the rings to extend. Conversely, one might expect a similar behavior for the 6^3_2 configuration, but counterintuitively, the 6^3_1 configuration exhibits a higher L^2/R_g^2 than the 6^3_2 configuration, even when every ring is constrained to two other rings separately. On the other hand, in Fig. 7(d), confined systems exhibit similar trends, but collapse occurs at a lower λ . Notably, at $\lambda=0$, the 6^3_1 configuration has a higher L^2/R_g^2 value than even 6^3_3 , presenting a non-trivial result that warrants further investigation.

To characterize the complexity of entanglements within each link, we compute the average crossing number (ACN). The crossing number counts the number of times one part of the link crosses over another when the link is projected onto a specific plane; the ACN measures this quantity projected over all possible planes. The ACN will always be greater than the invariant minimum crossing number and is typically anti-correlated with the radius of gyration, as a more compact configuration will contain more folded sections of the molecule. The formula to calculate the ACN is⁷⁴

$$ACN = \frac{1}{4\pi} \int_{\gamma_i} \int_{\gamma_j} \frac{|\hat{\boldsymbol{r}} \cdot d\boldsymbol{r}_i \times d\boldsymbol{r}_j|}{|\boldsymbol{r}_i - \boldsymbol{r}_j|^2}, \tag{7}$$

where γ_i and γ_j are the contours of the rings, and \mathbf{r}_i and \mathbf{r}_j are the respective spatial 3D coordinates.

As shown in Fig. 8, the ACN increases with the topological complexity of the links, as expected, and rises as self-interactions within the molecule induce a more compact state. Under confine-

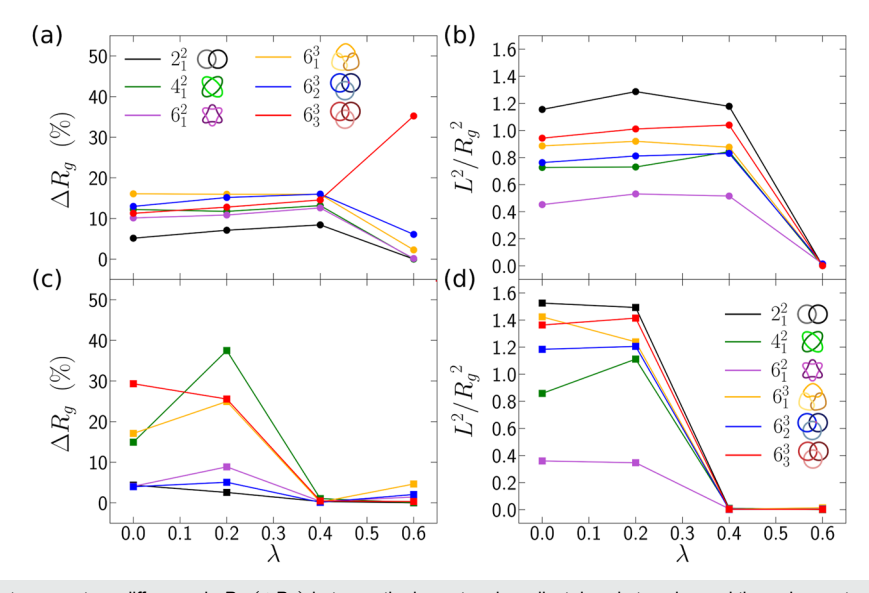


FIG. 7. Time-averaged absolute percentage difference in R_g (ΔR_g) between the largest and smallest rings in two-ring and three-ring systems with different conformational topologies (labeled with Alexander–Briggs notation 57) as a function of the interaction parameter λ (a) without confinement and (c) in slit-like confinement. Normalized mean-squared ring center-to-center distance L^2/R_g^2 as a function of the interaction parameter λ (b) without confinement and (d) in slit-like confinement. Note that $\lambda=0.6$ results are presented only for completeness; those systems are collapsed into compact shapes that are kinetically trapped in a certain way depending on the initial conditions and do not represent equilibrium states.

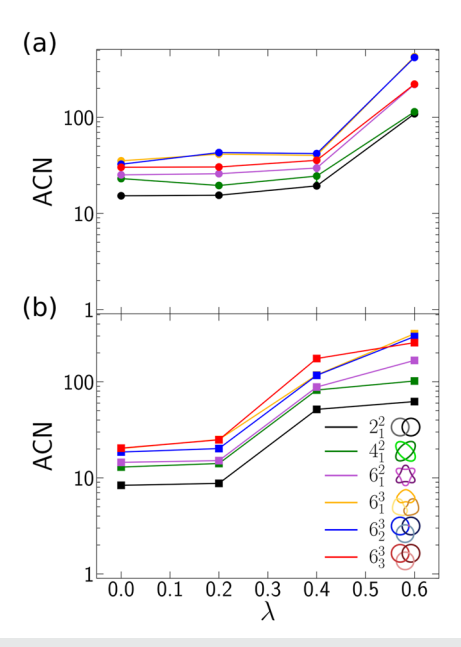


FIG. 8. Average crossing number (ACN) as a function of the interaction parameter λ for various topological conformations (labeled with Alexander–Briggs notation⁵⁷) (a) without confinement and (b) in slit-like confinement. The bars show the standard errors of all the measurements. Note that $\lambda=0.6$ results are presented only for completeness; those systems are collapsed into compact shapes that are kinetically trapped in a certain way depending on the initial conditions and do not represent equilibrium states.

ment in good solvent conditions, the links are effectively flattened closer to their minimum-crossing configurations when projected onto most planes, giving an ACN close to their minimum crossing number. Two linked circles would have an ACN slightly above 2, as they cross twice in most projections but more times when viewed obliquely from the side. Two linked ring polymers, such as the $\lambda = 0.0~2_1^2$ configurations in Fig. 3, would have a higher average crossing number because the entropic folding of the polymer leads to crossings, as shown in many projections. A higher value, toward 100, indicates that the different strands wind around each other many times, such that there is no projection in which the polymer does not cross itself dozens or hundreds of times. In that sense, it is a topological indicator of the polymer's compaction.

IV. CONCLUSION

We conducted MD simulations to investigate the impact of molecular topological linkage and the effect of slit-like nanoconfinement on the conformational properties under varying solvent qualities of fundamental linked-ring polymers comprising two and three rings. Our coarse-grained model is based on the Kremer–Grest model for modeling polymers, with parameters designed to mimic the physical features of the minirings that make up kDNA networks

In good-quality solvents and for two-ring systems, molecules with a higher number of crossing points (a more internally constrained structure) yield smaller average values of the mean radius of gyration and make for a softer flat-to-collapse transition (a smaller

change in radius of gyration upon transition). This phenomenon holds in both non-confined and nanoconfined systems. However, this same phenomenon is not observed in the three-ring systems studied. For the types of linkages studied here, the three rings could always move away from each other (in terms of their centers of mass) by concentrating the crossings at a common region in the middle of the structure, while each ring could extend away from this small region. The understanding that behaviors observed in two-ring systems may differ from those in three-ring systems provides insights that extrapolating behavior from single molecule analysis to large catenated networks, such as kDNA, is nontrivial.

In poor-quality solvents, structures tend to collapse, resulting in overall compact configurations with increased contacts. This leads to diverse morphological structures determined more by the topological linkage than the number of rings.

It is worth noting that, consistent with experimental results for kDNA networks, extreme confinement induces more isotropic and extended conformations for catenated polymers. In this scenario, links are effectively flattened into their minimum-crossing configurations when projected onto most planes. In addition, the flat-to-collapse transition in extreme confinement occurs at lower values of λ compared to non-confined systems.

Future efforts will be extended to investigate the threshold at which solvent quality can potentially induce kinetically trapped states in simulations and, likely, experiments as solvent strength is decreased by testing more values of λ for particular conformations. Finally, to achieve a more detailed understanding of the single-molecule behavior of catenated DNA chains, we could model these molecules with a worm-like chain model, introducing torsional potentials and the characteristic twist present in DNA, as in our previous work. The DNA would allow for a closer representation of this molecule and its longer ranged interactions. From this understanding, we can also extend to larger networks to approach a kDNA system.

SUPPLEMENTARY MATERIAL

See the supplementary material for additional details and analyses on single isolated rings and linear polymer chains as baseline cases for comparative purposes with the catenanes in the main text, and multiple simulations on single molecule systems at high λ to analyze kinetically trapped conformations (snapshots provided).

ACKNOWLEDGMENTS

This work was supported by the Cal. State. Long Beach and Ohio State University Partnership for Education and Research in Hard and Soft Materials, a National Science Foundation PREM, under Grant No. 2122199. We also acknowledge the Ohio Supercomputer Center for high-performance computing resources (http://osc.edu/ark:/19495/f5s1ph73).⁷⁷

AUTHOR DECLARATIONS

Conflict of Interest

The authors have no conflicts to disclose.

Author Contributions

Diego Becerra: Conceptualization (equal); Methodology (equal); Supervision (equal); Writing - original draft (equal); Writing review & editing (equal). Alexander R. Klotz: Conceptualization (equal); Writing - review & editing (supporting). Lisa M. Hall: Conceptualization (equal); Methodology (equal); Supervision (equal); Writing - review & editing (equal).

DATA AVAILABILITY

The data that support the findings of this study are available from the corresponding author upon reasonable request.

REFERENCES

- ¹J.-P. Sauvage and C. Dietrich-Buchecker, Molecular Catenanes, Rotaxanes and Knots: A Journey Through the World of Molecular Topology (John Wiley & Sons,
- ²D. Sluysmans and J. F. Stoddart, "The burgeoning of mechanically interlocked molecules in chemistry," Trends Chem. 1, 185-197 (2019).
- ³ J. Prentis, "Spatial correlations in a self-repelling ring polymer," J. Chem. Phys. **76**, 1574–1583 (1982).
- ⁴A. Y. Grosberg, "Critical exponents for random knots," Phys. Rev. Lett. **85**, 3858
- ⁵T. E. Gartner III, F. M. Haque, A. M. Gomi, S. M. Grayson, M. J. Hore, and A. Jayaraman, "Scaling exponent and effective interactions in linear and cyclic polymer solutions: Theory, simulations, and experiments," Macromolecules 52, 4579-4589 (2019).
- ⁶M. Müller, J. Wittmer, and M. Cates, "Topological effects in ring polymers: A computer simulation study," Phys. Rev. E 53, 5063 (1996).
- ⁷M. Müller, J. Wittmer, and M. Cates, "Topological effects in ring polymers. II. Influence of persistence length," Phys. Rev. E 61, 4078 (2000).
- ⁸M. Q. Tu, O. Davydovich, B. Mei, P. K. Singh, G. S. Grest, K. S. Schweizer, T. C. O'Connor, and C. M. Schroeder, "Unexpected slow relaxation dynamics in pure ring polymers arise from intermolecular interactions," ACS Polym. Au 3, 307-317 (2023).
- ⁹T. C. O'Connor, T. Ge, M. Rubinstein, and G. S. Grest, "Topological linking drives anomalous thickening of ring polymers in weak extensional flows," Phys. Rev. Lett. 124, 027801 (2020).
- ¹⁰T. C. O'Connor, T. Ge, and G. S. Grest, "Composite entanglement topology and extensional rheology of symmetric ring-linear polymer blends," J. Rheol. 66, 49-65 (2022).
- ¹¹K. Hagita, T. Murashima, and N. Sakata, "Mathematical classification and rheological properties of ring catenane structures," Macromolecules 55, 166-177
- ¹²R. Staňo, C. N. Likos, and S. A. Egorov, "Mixing linear polymers with rings and catenanes: Bulk and interfacial behavior," Macromolecules 56, 8168-8182
- 13 R. Staňo, C. N. Likos, and J. Smrek, "To thread or not to thread? Effective potentials and threading interactions between asymmetric ring polymers," Soft Matter **19**, 17–30 (2023).
- ¹⁴L. Tubiana, F. Ferrari, and E. Orlandini, "Circular polycatenanes: Supramolecular structures with topologically tunable properties," Phys. Rev. Lett. 129, 227801
- ¹⁵J. Roovers and P. Toporowski, "Synthesis of high molecular weight ring
- polystyrenes," Macromolecules **16**, 843–849 (1983). ¹⁶A. Takano, Y. Ohta, K. Masuoka, K. Matsubara, T. Nakano, A. Hieno, M. Itakura, K. Takahashi, S. Kinugasa, D. Kawaguchi et al., "Radii of gyration of ring-shaped polystyrenes with high purity in dilute solutions," Macromolecules 45, 369-373 (2012).
- ¹⁷P. He, A. J. Katan, L. Tubiana, C. Dekker, and D. Michieletto, "Single-molecule structure and topology of kinetoplast DNA networks," Phys. Rev. X 13, 021010 (2023).

- 18 Q. Wu, P. M. Rauscher, X. Lang, R. J. Wojtecki, J. J. De Pablo, M. J. Hore, and S. J. Rowan, "Poly[n] catenanes: Synthesis of molecular interlocked chains," Science 358, 1434-1439 (2017).
- $^{19}\mbox{S.-S.}$ Jester and M. Famulok, "Mechanically interlocked DNA nanostructures for functional devices," Acc. Chem. Res. 47, 1700-1709 (2014).
- ²⁰C. Mao, W. Sun, N. C. Seeman et al., "Assembly of Borromean rings from DNA," Nature 386, 137-138 (1997).
- ²¹Y. Weizmann, A. B. Braunschweig, O. I. Wilner, Z. Cheglakov, and I. Willner, "A polycatenated DNA scaffold for the one-step assembly of hierarchical nanostructures," Proc. Natl. Acad. Sci. U. S. A. 105, 5289-5294 (2008).
- ²²T. L. Schmidt and A. Heckel, "Construction of a structurally defined doublestranded DNA catenane," Nano Lett. 11, 1739-1742 (2011).
- ²³S. Erbas-Cakmak, D. A. Leigh, C. T. McTernan, and A. L. Nussbaumer, "Artificial molecular machines," Chem. Rev. 115, 10081-10206 (2015).
- ²⁴A. Harada, "Cyclodextrin-based molecular machines," Acc. Chem. Res. 34, 456-464 (2001).
- ²⁵J. Chen and N. C. Seeman, "Synthesis from DNA of a molecule with the connectivity of a cube," Nature 350, 631-633 (1991).
- ²⁶R. P. Goodman, I. A. Schaap, C. F. Tardin, C. M. Erben, R. M. Berry, C. F. Schmidt, and A. J. Turberfield, "Rapid chiral assembly of rigid DNA building blocks for molecular nanofabrication," Science 310, 1661-1665 (2005).
- ²⁷J. Chen, P. T. Englund, and N. R. Cozzarelli, "Changes in network topology during the replication of kinetoplast DNA," EMBO J. 14, 6339-6347 (1995).
- ²⁸J. Chen, C. A. Rauch, J. H. White, P. T. Englund, and N. R. Cozzarelli, "The topology of the kinetoplast DNA network," Cell 80, 61-69 (1995).
- ²⁹ A. R. Klotz, B. W. Soh, and P. S. Doyle, "Equilibrium structure and deformation response of 2D kinetoplast sheets," Proc. Natl. Acad. Sci. U. S. A. 117, 121-127
- 30 J. Lukeš, D. Lys Guilbride, J. Votýpka, A. Zíková, R. Benne, and P. T. Englund, "Kinetoplast DNA network: Evolution of an improbable structure," Eukaryotic Cell 1, 495-502 (2002).
- $^{\bf 31}{\rm T.}$ A. Shapiro and P. T. Englund, "The structure and replication of kinetoplast DNA," Annu. Rev. Microbiol. 49, 117-143 (1995).
- 32 I. Yadav, D. Al Sulaiman, B. W. Soh, and P. S. Doyle, "Phase transition of catenated DNA networks in poly(ethylene glycol) solutions," ACS Macro Lett. 10, 1429-1435 (2021).
- ³³L. Simpson, "Structure and function of kinetoplast DNA," J. Protozool. 20, 2–8
- ³⁴M. Laurent and M. Steinert, "Electron microscopy of kinetoplastic DNA from trypanosoma mega," Proc. Natl. Acad. Sci. U. S. A. 66, 419-424 (1970).
- ³⁵J. Shlomai and A. Zadok, "Reversible decatenation of kinetoplast DNA by a DNA topoisomerase from trypanosomatids," Nucleic Acids Res. 11, 4019-4034 (1983).
- ³⁶D. L. Pérez-Morga and P. T. Englund, "The attachment of minicircles to kinetoplast DNA networks during replication," Cell 74, 703-711 (1993).
- ³⁷J. Shlomai, "The assembly of kinetoplast DNA," Parasitol. Today 10, 341–346 (1994).
- ³⁸J. C. Morris, M. E. Drew, M. M. Klingbeil, S. A. Motyka, T. T. Saxowsky, Z. Wang, and P. T. Englund, "Replication of kinetoplast DNA: An update for the new millennium," Int. J. Parasitol. 31, 453-458 (2001).
- 39 B. Liu, Y. Liu, S. A. Motyka, E. E. Agbo, and P. T. Englund, "Fellowship of the rings: The replication of kinetoplast DNA," Trends Parasitol. 21, 363-369
- ⁴⁰N. Yaffe, D. Rotem, A. Soni, D. Porath, and J. Shlomai, "Direct monitoring of the stepwise condensation of kinetoplast DNA networks," Sci. Rep. 11, 1501 (2021).
- ⁴¹B. W. Soh and P. S. Doyle, "Equilibrium conformation of catenated DNA networks in slitlike confinement," ACS Macro Lett. 10, 880-885 (2021).
- ⁴²J. M. Polson, E. J. Garcia, and A. R. Klotz, "Flatness and intrinsic curvature of linked-ring membranes," Soft Matter 17, 10505-10515 (2021).
- ⁴³H. Sugisaki and D. S. Ray, "DNA sequence of *Crithidia fasciculata* kinetoplast minicircles," Mol. Biochem. Parasitol. 23, 253-263 (1987).
- ⁴⁴L. Simpson and A. da Silva, "Isolation and characterization of kinetoplast DNA from Leishmania tarentolae," J. Mol. Biol. 56, 443-473 (1971).

- ⁴⁵D. Michieletto, D. Marenduzzo, and E. Orlandini, "Is the kinetoplast DNA a percolating network of linked rings at its critical point?," Phys. Biol. **12**, 036001 (2015).
- ⁴⁶C. A. Rauch, D. Perez-Morga, N. R. Cozzarelli, and P. T. Englund, "The absence of supercoiling in kinetoplast DNA minicircles," EMBO J. 12, 403–411 (1993).
- ⁴⁷T. Li, H. Zhang, L. Hu, and F. Shao, "Topoisomerase-based preparation and AFM imaging of multi-interlocked circular DNA," Bioconjugate Chem. 27, 616–620 (2016).
- ⁴⁸D. G. Ferschweiler, R. Blair, and A. R. Klotz, "Percolation and dissolution of Borromean networks," Phys. Rev. E **107**, 024304 (2023).
- ⁴⁹ A. Y. Grosberg, "Do knots self-tighten for entropic reasons?," Polym. Sci., Ser. A 58, 560–568 (2016).
- ⁵⁰G. Amici, M. Caraglio, E. Orlandini, and C. Micheletti, "Topologically linked chains in confinement," ACS Macro Lett. 8, 442–446 (2019).
- ⁵¹G. Amici, M. Caraglio, E. Orlandini, and C. Micheletti, "Topological friction and relaxation dynamics of spatially confined catenated polymers," ACS Macro Lett. 11, 1–6 (2021).
- ⁵²T. Zhang, K. I. Winey, and R. A. Riggleman, "Conformation and dynamics of ring polymers under symmetric thin film confinement," J. Chem. Phys. 153, 184905 (2020).
- ⁵³ P. Kuterba, Z. Danel, and W. Janke, "Entropic force in a dilute solution of real ring polymer chains with different topological structures in a slit of two parallel walls with mixed boundary conditions," Condens. Matter Phys. 26, 43605 (2023).
 ⁵⁴ M. Rubinstein and R. Colby, Polymer Physics (Oxford University Press, New
- York, 2003).

 55 H. Guo, K. Ojan, and M. Tsige, "Theta temperature depression of mechani-
- ⁵⁵H. Guo, K. Qian, and M. Tsige, "Theta temperature depression of mechanically interlocked polymers: [2]catenane as a model polymer," Macromolecules 56, 9164–9174 (2023).
- ⁵⁶D. A. Holling, "Measuring the Flory exponent of double sized kinetoplasts and observing the 2D version of a coil-globule transition," M.Sc. thesis (California State University, Long Beach, 2023), available from ProQuest Dissertations & Theses A&I; ProQuest Dissertations & Theses Global; Publicly Available Content Database (2892615102).
- ⁵⁷C. J. Bruns and J. F. Stoddart, The Nature of the Mechanical Bond: From Molecules to Machines (John Wiley & Sons, 2016).
- ⁵⁸D. Rolfsen, in *Knots and Links, Mathematical Lecture Series Vol. 15* (Publish or Perish, Inc., Berkeley, CA, 1976), pp. 6–7.
- ⁵⁹D. Rolfsen, *Knots and Links* (American Mathematical Society, 2003), Vol. 346.
- ⁶⁰G. S. Grest and K. Kremer, "Molecular dynamics simulation for polymers in the presence of a heat bath," Phys. Rev. A 33, 3628 (1986)
- presence of a heat bath," Phys. Rev. A 33, 3628 (1986).

 61 K. Kremer and G. S. Grest, "Dynamics of entangled linear polymer melts: A molecular-dynamics simulation," J. Chem. Phys. 92, 5057–5086 (1990).

- ⁶² J. D. Weeks, D. Chandler, and H. C. Andersen, "Role of repulsive forces in determining the equilibrium structure of simple liquids," J. Chem. Phys. **54**, 5237–5247 (1971).
- ⁶³ J.-P. Hansen and I. R. McDonald, *Theory of Simple Liquids: With Applications to Soft Matter* (Academic Press, 2013).
- ⁶⁴S. Huissmann, R. Blaak, and C. N. Likos, "Star polymers in solvents of varying quality," Macromolecules 42, 2806–2816 (2009).
- ⁶⁵H. Yagyu, J.-Y. Lee, D.-N. Kim, and O. Tabata, "Coarse-grained molecular dynamics model of double-stranded DNA for DNA nanostructure design," J. Phys. Chem. B **121**, 5033–5039 (2017).
- ⁶⁶M. Caraglio, C. Micheletti, and E. Orlandini, "Mechanical pulling of linked ring polymers: Elastic response and link localisation," Polymers 9, 327 (2017).
 ⁶⁷A. P. Thompson, H. M. Aktulga, R. Berger, D. S. Bolintineanu, W. M. Brown,
- ⁶⁷ A. P. Thompson, H. M. Aktulga, R. Berger, D. S. Bolintineanu, W. M. Brown, P. S. Crozier, P. J. in't Veld, A. Kohlmeyer, S. G. Moore, T. D. Nguyen, R. Shan, M. J. Stevens, J. Tranchida, C. Trott, and S. J. Plimpton, "LAMMPS—A flexible simulation tool for particle-based materials modeling at the atomic, meso, and continuum scales," Comput. Phys. Commun. 271, 108171 (2022).
- ⁶⁸ M. D. Hanwell, D. E. Curtis, D. C. Lonie, T. Vandermeersch, E. Zurek, and G. R. Hutchison, "Avogadro: An advanced semantic chemical editor, visualization, and analysis platform," J. Cheminf. **4**, 17 (2012).
- ⁶⁹P.-G. de Gennes (1999). "Flexible polymers in nanopores," In: Granick, S., et al. Polymers in Confined Environments. Advances in Polymer Science, (Springer, Berlin, Heidelberg) vol. 138 (1999).
- ⁷⁰T. Odijk, "The statistics and dynamics of confined or entangled stiff polymers," Macromolecules **16**, 1340–1344 (1983).
- ⁷¹P. M. Rauscher, K. S. Schweizer, S. J. Rowan, and J. J. De Pablo, "Thermodynamics and structure of poly[*n*]catenane melts," Macromolecules **53**, 3390–3408 (2020).
- ⁷²L. Dai, J. J. Jones, A. R. Klotz, S. Levy, and P. S. Doyle, "Nanoconfinement greatly speeds up the nucleation and the annealing in single-DNA collapse," Soft Matter 13, 6363–6371 (2017).
- ⁷³D. N. Theodorou and U. W. Suter, "Shape of unperturbed linear polymers: Polypropylene," <u>Macromolecules</u> 18, 1206–1214 (1985).
- ⁷⁴R. G. Scharein, "Interactive topological drawing," Ph.D. thesis, Department of Computer Science, The University of British Columbia, 1998.
- ⁷⁵D. Becerra, P. R. Jois, and L. M. Hall, "Coarse-grained modeling of polymers with end-on and side-on liquid crystal moieties: Effect of architecture," J. Chem. Phys. 158, 224901 (2023).
- ⁷⁶D. Becerra, Y. Xu, X. Wang, and L. M. Hall, "Impact of molecular-level structural disruption on relaxation dynamics of polymers with end-on and side-on liquid crystal moieties," ACS Nano 17, 24790–24801 (2023).
- Ohio Supercomputer Center. (1987); http://osc.edu/ark:/19495/f5s1ph73